Effect of Inlet Turbulence on Compressor Noise

B. Robbins* and B. Lakshminarayana†
The Pennsylvania State University, University Park, Pa.

The sound generated by the interaction of inlet turbulence with a rotating compressor blade row is investigated. Currently, there are two theories relating the rotor geometry and blade aerodynamics to the spectrum of the radiated sound. These theories are extended to include the cascade effect by incorporating a cascade aerodynamic response function for the unsteady lift on the blades into their analyses. To experimentally study this noise source, an aeroacoustic compressor facility was designed and built. The parameters investigated include turbulence intensity and longitudinal integral length scale, blade speed, flow coefficient. The results indicate a definite increase in the overall sound pressure level and an increase in the spectrum level of the sound pressure with an increase in turbulence intensity. For integral length scales smaller than the blade spacing, the total sound power is found to be proportional to (turbulence velocity/integral length),^{2} where turbulence velocity is rms value normal to the blade chord. Comparison of theoretical results with experimental data indicates one theory to predict the sound pressure level fairly accurately in a limited frequency range.

Nomenclature

a_o = speed of sound
B = number of rotor blades
$2b$, c = blade chord length
$F_1(R/\Lambda_f, kR)$ = radiation function given in Ref. 3
f = frequency in hertz
$g(\Gamma)$ = frequency parameter
$H(\omega,\sigma,\xi)$ = cascade aerodynamic response function
I = sound intensity in w/ft^2
k = χS, nondimensional wavenumber
k_x, k_y = axial and tangential components (Absolute System) of k
M_a = U_x/a_o, axial flow Mach number
M_r = flow Mach number relative to the rotor
M_t = rotor tip Mach number
n = integer
$(\overline{q^2})^{1/2}$ = rms value of turbulence velocity normal to the blade chord
R = rotor tip radius
r_h/R = hub-to-tip ratio
S = blade spacing
U_{rel} = $(U_x^2 + V^2)^{1/2}$, flow velocity relative to the rotor
U_x = axial flow velocity
u = turbulent fluctuating velocity in the axial direction
v = turbulent fluctuating velocity in the tangential direction
V = rotor blade speed
W = sound power in w
Γ = $2\pi f\Lambda_f/U_x$, nondimensional frequency
δ_r = spanwise distance along the blade
Λ_f = longitudinal integral length scale of the turbulence
ν = frequency in rad/sec
ξ = cascade stagger angle
ρ = fluid density
σ = c/S, blade row solidity
τ = intrablade phase angle in rad/sec
ϕ = U_x/V, flow coefficient
χ = $2\pi f/a_o$, acoustic wavenumber
ω = $\nu c/2U_{rel}$, reduced frequency
$\omega_r\pm$ = $\dfrac{c\chi}{2M_r(1-M_a^2)^{1/2}}\{(1-M_a^2)^{1/2} \pm M_t\}$
λ = wavelength of sound

Presented as Paper 74-265 at the AIAA 10th Annual Meeting and Technical Display; submitted November 15, 1973; revision received March 6, 1974. The research contained in this paper was performed under the sponsorship of the Applied Research Laboratory of The Pennsylvania State University, which operates under contract with the Naval Ordnance Systems Command. The authors wish to express their gratitute to M. Sevik for his help in initiating this study, to G. Reethof and D. E. Thompson for their helpful suggestions in making the acoustical measurements, and to R. Mani for making available the computer programs used in this investigation. B. Robbins wishes to express his gratitute to the National Aeronautics and Space Administration for the award of a NASA Acoustics Traineeship.

Index categories: Noise, Powerplant Aircraft; Nonsteady Aerodynamics; Air Breathing Propulsion, Subsonic and Supersonic.

*NASA Acoustics Trainee, presently at Pratt & Whitney Aircraft Company, East Hartford, Conn. Associate Member AIAA.

†Associate Professor of Aerospace Engineering, Applied Research Lab. Associate Fellow AIAA.

1. Introduction

SINCE the development of turbojet-powered commercial aircraft, the noise level near major airports has greatly increased. Noise from the jet exhaust was reduced by using higher by-pass ratio engines and modified exhaust nozzles. It then became apparent that during takeoff and landing the primary source of noise could be attributed to the engine compressor or fan. Therefore, identification of the noise sources within the fan is an important step in reducing this noise problem.

It is known that the noise radiated from turbomachinery consists of a broadband signal on which a number of discrete peaks are superimposed. These characteristics of the radiated sound spectrum have been observed on fans, aircraft compressors, and marine propellers. The generation of broadband sound suggests processes that are random in nature. Recent studies have found four major sources of broadband fan noise; blade boundary layers, separated flows as in stall, vortex shedding from the blade trailing edge and lastly, the freesteam turbulence in the inlet flow. The last effect, which could be one of the more significant noise generators, is studied in this investigation.

The mechanisms by which the incident turbulence, both in an upstream wake and in the freestream, generate noise are twofold:

1) *Quadrupole Sources.* The turbulence provides a mechanism by which the potential flowfield around the rotor is scattered as sound. Ffowcs-Williams and Hawkings[1] first pointed out this effect, and later, Chandrashekara[2] investigated the significance of these sources in detail. The investigations carried out so far indicate that these quadrupole sources are insignificant noise generators at low Mach numbers and low blade loading.

2) *Dipole Sources.* The nonuniform velocity field associated with turbulence produces fluctuations in the angle of

attack to the blade row, leading to unsteady blade forces and, hence, noise generation. This gives rise to dipole sources on the blade surfaces. Sevik[3] and Mani[4] investigated this effect, theoretically, using Sears'[5] function for the calculation of the unsteady blade forces generated by the inlet turbulence. The objective of this paper is to study this source of noise, which is likely to be dominant.

The experimental evidence (qualitative) on the dependency of radiated sound intensity on inlet turbulence is due to Sofrin and McCann.[6] They examined the noise due to inlet guide vane (IGV) and rotor viscous interaction as a function of axial spacing between IGV and rotor. A fall off in the noise level is observed with increasing spacing, up to a certain spacing, and then it leveled off. Whereas, the noise level decreased much further with the removal of IGV. Sofrin and McCann conclude that the presence of IGV upstream of the rotor raises the turbulence level in the duct, and the drop off in noise level on complete removal of the IGV's is due to lowering of turbulence incident on the rotor. Quantitative measurement of the sound intensity due to incident turbulence is not available. This is one of the objectives of this program.

At the present time, there is no data available to substantiate the theories proposed on the quantitative effects of dipole sources in sound generation. In addition to checking these theories, it is the intention of this investigation to gain some basic information on the interaction of inlet turbulence with the flow and blade parameters in producing the acoustic field. An understanding of these detailed mechanisms may ultimately lead to noise reduction techniques. The parameters effecting the acoustic field produced by freestream turbulence and rotor interaction are studied in this paper. Specifically, these parameters include the turbulence intensity, the ratio of the integral length scale of the turbulence to the blade spacing, and the flow coefficient.

In order to acquire the necessary information, a compressor noise facility was designed and built by the authors. The inlet turbulence was generated by three square mesh grids of different sizes. The relevant flow parameters are measured experimentally. Then, spectral measurements of the sound radiation were made; these include measurements made by both a 10 Hz and a ⅓-octave band wave analyzer. Further, the spectral content of the directivity patterns were made with a ⅓-octave filter. The theories were then compared with the experimental data.

2. Theoretical Considerations

Previous theoretical investigations of dipole sound radiation due to the operation of a rotor in a turbulent inflow have been carried out by Sevik[3] and Mani.[4]

In Sevik's analysis the turbulent inflow is assumed to be homogeneous and isotropic. The lift fluctuations over a typical blade are determined. The correlation of these time-dependent lift is related to the spatial and temporal correlation of the velocity fluctuations in the approach stream. The aerodynamic response function was chosen to be that developed by Sears.[5] This function is based on two-dimensional, incompressible, thin-airfoil aerodynamics and ignores mutual interference between blade elements. A further simplification is made in that the Sears' function is chosen as the mean value for the entire blade span. The spectral density of the radiated sound due to the fluctuating lift on the blades is determined. The effects of rotor ducting on the radiated sound are not considered and acoustic compactness of the blades is assumed. In addition, it is assumed that the solidity of the rotor is such that it can be treated acoustically as a disk, which implies that the acoustic wavelength must be much larger than the blade chord and the blade spacing.

Sevik's theory predicts that the radiated sound spectrum depends on such parameters as the turbulence level, a characteristic time scale derived from the ratio of the integral scale of the turbulence divided by the axial flow velocity, and characteristic length scales such as the ratio of the integral scale of the turbulence to the acoustic wavelength, the radius of the rotor and the blade chord. Sevik's theory does not include blade-to-blade correlations of the time-dependent lift and hence, the resulting spectra do not exhibit a broadband peak centered at the blade passing frequency and multiples. Sevik's derivation yielded the following expression for the spectral density of the sound power:

$$\frac{dW}{d\Gamma} = \frac{\pi^2}{2}\left(\frac{\overline{u^2}}{U_x^2}\right) M_a^3 \left(\frac{\rho U_x^3 R^2}{1+\phi^2}\right)\left(\frac{R}{\Lambda_f}\right)^2\left[1-\left(\frac{r_h}{R}\right)^2\right]^2 g(\Gamma) F_1\left(\frac{R}{\Lambda_f}, kR\right) \tag{1}$$

where

$\Gamma = 2\pi f \Lambda_f / U_x$ nondimensional frequency

W = sound power in watts

U_x = axial velocity

R = rotor tip radius

Λ_f = longitudinal integral length scale of the turbulence

$F_1(R/\Lambda_f, kR)$ = radiation function given in (Ref. 3)

M_a = axial Mach number,

ϕ = flow coefficient

r_h/R = hub-to-tip ratio

f = frequency in hertz

$g(\Gamma)$ is the frequency dependent term in the spectrum of the total normal force acting on the blade and Sevik's expression for $g(\Gamma)$ is

$$g(\Gamma) = \frac{\Gamma^2}{1+\Gamma^2}\left[\frac{1}{1+2\pi\omega}\right]\left(2\left(1+\frac{1}{\phi^2}\right)+\frac{1-\Gamma^2}{1+\Gamma^2}\right) \tag{2}$$

where ω is the reduced frequency and is equal to $\nu c/2U_{\text{rel}}$.

The term in the square bracket of Eq. (2) represents an approximation to Sears'[5] function $[S(\omega)]^2 \simeq (1+2\pi\omega)^{-1}$. In the present investigation, Sears' function is replaced by a cascade gust function, which takes into account the interference effect due to adjoining blades in a cascade. If this is represented by $H(\omega,\sigma,\xi)$, where ξ is the blade stagger angle and σ is the solidity of the blades, the resulting expression for $g(\Gamma)$ is

$$g(\Gamma) = \frac{\Gamma^2}{1+\Gamma^2}[H(\omega,\sigma.\xi)]^2\left(2\left(1+\frac{1}{\phi^2}\right)+\frac{1-\Gamma^2}{1+\Gamma^2}\right) \tag{3}$$

Use of the cascade gust function $H(\omega,\sigma,\xi)$, in place of Sears' function, is intended to refine Sevik's (Eq. 1) and Mani's theory (described later) by including the cascade effect. There have been several investigations dealing with the unsteady forces generated in a cascade, due to blade vibrations and upstream unsteadiness in the flow. Hanamura[7] treated the unsteady flow through large cambered blades in a cascade and Whitehead[8] carried out a similar analysis for a cascade of flat plates. Both of these investigations are based on the method of singularities and are probably the most accurate analyses available to date. In the present investigation, Whitehead's[8] analysis is used to derive the values of $H(\omega,\sigma,\xi)$‡ for the rotor used by the authors.

Mani[4] carried out an analysis relating the characteristics of the turbulence and design parameters of the rotor to the spectrum of the radiated sound. He used a spectral

‡This function corresponds to Whitehead's aerodynamic coefficient C_{FW}.

representation of the turbulence, regarding the turbulence as a super-position of shear waves. It is assumed that the turbulence is homogeneous, isotropic, and weakly stationary, and that the longitudinal velocity correlation is of the type $\exp(-r/\Lambda_f)$ where r is the separation between points in the turbulent field and Λ_f is the length scale of the turbulence. Mani employs the aerodynamic response function developed by Sears,[5] consequently, the effects of adjoining blades in the rotor on the time-dependent blade forces are not accounted for.

In the determination of the radiated sound spectrum, only waves above the cutoff frequency are regarded as contributing to the far-field acoustic energy and reflections from open ends of ducts and adjacent blade rows are neglected. The sound radiation upstream and downstream of the blade row is computed. The results show that the amount of acoustic energy per unit frequency, as a function of frequency, is obtained as a function of the axial flow Mach number, blade tip speed, blade row solidity, turbulence intensity, and of the ratio of the length scale Λ_f of the turbulence to the transverse separation between the blades S. The spectrum contains broadband peaks at blade passing frequency and multiples as long as Λ_f/S exceeds about 0.5. For larger values of Λ_f/S, the peaks become sharper. For $\Lambda_f/S = 0.1$, computed by Mani, the spectrum shows no peaks at the blade passing frequency. Although the peaks disappear for small values of Λ_f/S, the nondimensional sound levels increase as Λ_f/S becomes smaller. Mani's expression for the spectral density of the sound intensity is

$$\chi\frac{dI}{d\chi} = \frac{3}{2}\rho U_x \overline{u^2}\cdot\frac{\pi^2\sigma^2\chi S}{24\Lambda_f\cos^2\xi}\cdot \left[\frac{(1-M_a^2)^{1/2}}{2\pi c\chi\sin\xi}\log\left\{\frac{1+2\pi\omega_{r+}}{1+2\pi\omega_{r-}}\right\}\right]\cdot \left\{\int\frac{(1+3\cos^2\xi)k_x^2 + \Lambda_f^{-2} + 6k_xk_y\cos\xi\sin\xi + (1+3\sin^2\xi)k_y^2}{(\Lambda_f^{-2}+k_x^2+k_y^2)^{1/2}}\,dk_y\right\}\cdot \sin^2\xi\left\{\frac{\pi}{2} + \frac{(1-M_a^2)(\cot^2\xi-1)}{2}\cdot\left(-\frac{\pi}{2M_a^2} + \frac{\pi}{2M_a^2(1-M_a^2)^{1/2}} - \left\{\frac{\arcsin M_a}{M_a^2(1-M_a^2)^{1/2}}\right\} + \frac{1}{M_a}\right)\right\} \tag{4}$$

where

I = sound intensity

χ = acoustic wavenumber

$U_{rel} = (U_x^2 + V^2)^{1/2}$, velocity relative to rotor

σ = solidity

$\omega_{r\pm} = \frac{c\chi}{2M_r(1-M_a^2)^{1/2}}\{(1-M_a^2)^{1/2} \pm M_t\}$

M_r, M_t = relative flow and blade tip Mach number respectively

$k = \chi S$

k_x, k_y = axial, tangential component of the nondimensional wavenumber k

The term in the square bracket of Eq. (4) is the average of Sears' function $[(S(\omega)]^2$, averaged over k_y. Here again, Mani uses the approximate form of Sears' function $[S(\omega)]^2 = (1 + 2\pi\omega)^{-1}$ and integrates this over k_y. For low Mach numbers, the term in the square bracket reduces to $(1 + 2\pi\omega)^{-1}$ as shown below.

For low Mach numbers, the expression in the square bracket of Eq. (4) can be written as

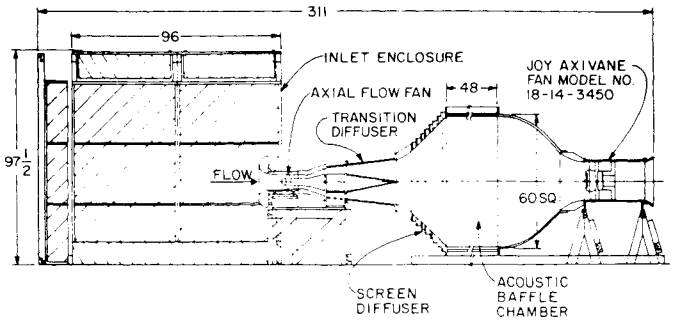

Fig. 1 Schematic of rotor noise facility (dimensions are in inches).

$$A = \frac{1}{2\pi\chi c\sin\xi}\log\left[\frac{1+\frac{\pi c\chi}{M_r}(1+M_t)}{1+\frac{\pi c\chi}{M_r}(1-M_t)}\right] = \frac{1}{2\pi\chi c\sin\xi}\log\left[\frac{1+\frac{M_t}{a}\frac{\pi c\chi}{M_r}}{1-\frac{M_t}{a}\frac{\pi c\chi}{M_r}}\right] \tag{5}$$

where

$$a = 1 + (\pi c\chi/M_r) = 1 + 2\pi\omega$$

For low tip Mach numbers (using the approximation $\log[(1+\epsilon)(1-\epsilon)^{-1}] \simeq 2\epsilon$ where ϵ is a small quantity)

$$A = \frac{1}{\sin\xi}\frac{M_t}{M_r}\frac{1}{a} = \frac{1}{1+2\pi\omega} = |S(\omega)|^2 \tag{6}$$

Mani's expression 4 can thus be modified (for low Mach numbers) to include the cascade effect by replacing the square bracket term in Eq. (4) by $|H(\omega,\sigma,\xi)|^2$. Here again, the authors have used Whitehead's[8] analysis to evaluate the cascade gust function $H(\omega,\sigma,\xi)$ for their rotor.

It is evident from Sevik and Mani's analyses that the acoustic power or intensity is a function of several variables

$$I \text{ or } W = f\left[\frac{\overline{u}^2}{U_x^2}, \omega, \frac{\Lambda_f}{S}, M_a, M_t, \phi, \sigma, H(\omega,\sigma,\xi)\right] \tag{7}$$

It is interesting to note that Sharland's[9] approximate expression,

$$W = \frac{\rho}{48\pi a_0^3}\int_{\text{SPAN}} C_{L_\alpha}{}^2 c U_{\text{rel}}{}^4\overline{u}^2 dy \tag{8}$$

takes into account some of these parameters. In this expression $C_{L\alpha}$ is the slope of the lift-angle of attack curve, which is taken into account in Sevik and Mani's analysis, modified by the authors, through the parameter $H(\omega,\sigma,\xi)$.

All these analyses indicate that I or W varies linearly with $\overline{u}^2$. In the experimental program described later, the parameters σ and ξ are held constant, and turbulence characteristics (such as $\overline{u}^2, \omega, \Lambda_f/S$) are varied. The flow parameters M_a, M_r, and ϕ are also varied, but not significantly.

3. Turbomachinery Noise Facility

An aeroacoustic compressor facility was designed and built by the authors to carry out the experimental investigation. A single stage axial flow compressor was used in this investigation. The facility consists of four main components: a large, acoustically treated enclosure surrounding the compressor inlet, the axial flow compressor, an acoustical baffle chamber downstream of the fan, and a Joy axial flow fan. A detailed drawing of the assembly is shown in Fig. 1.

The acoustical enclosure surrounding the fan inlet was designed to provide a known acoustical environment free

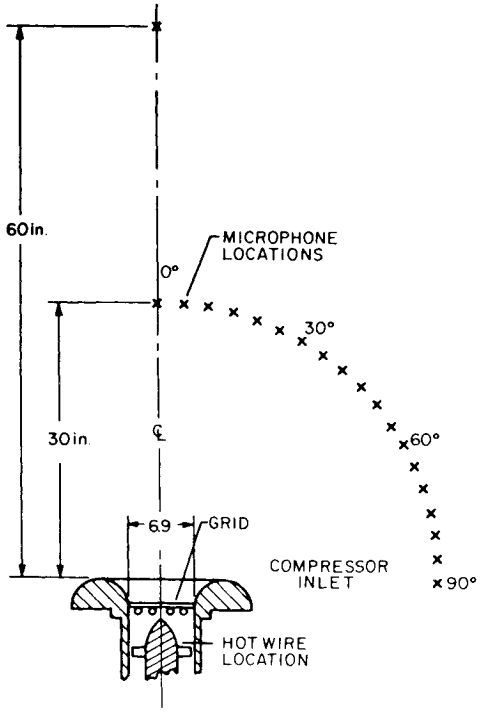

Fig. 2 Plan view showing microphone and hot wire locations.

of unknown sound reflections and reverberations. With limitations on its size, the inside dimensions of the chamber are 80.5, 96.0, and 76.0 in. in width, length, and height, respectively. Construction of the chamber is basically a wood frame, with side walls much like a bookcase; the spaces between the shelves being filled with Owens-Corning, Type 705, Industrial Fiberglas. The floor is covered with the same material. Fiberglass is suspended from the frame in wire mesh baskets; these baskets thus form the ceiling. The thickness of the acoustical treatment is 10 in. One end of the chamber is left open for the compressor inlet, but 2-in. thick fiberglass insulation is draped over most of the open area.

The inlet enclosure was calibrated using a known, but frequency limited, omnidirectional source. The variations in the sound pressure level (SPL) with distance on the centerline of the compressor axis were measured; in addition, the directivity of the sound field was obtained. The results indicate the chamber has anechoic conditions at frequencies above 1250 Hz. The directivity measurements indicated that the enclosure is omnidirectional above 630 Hz. Summarizing, the acoustical properties of the enclosure are known, and they become those of an anechoic chamber.

3.1 Rotor Characteristics

This section outlines the characteristics of the rotor which is employed in the noise facility. The hub-to-tip ratio of the rotor blades is 0.482. The tip diameter of the rotor is 6.90 in., and the hub diameter is 3.44 in. so that the blade span is 1.73 in. The chord is nearly constant (1.6 in.) from hub to tip. The stagger angle varies from 0.31 rad at the hub to 0.81 rad at the tip. The rotor is of free vortex design.

The standard configuration of the rotor employs 17 blades; the midspan blade spacing is 0.956 in. The range of steady velocities at the rotor inlet was from 97 to 142 fps. The rotor was operated in air at 3626, 4360, and 5440 rpm. The design lift coefficient of the rotor blade is 0.46 and the flow coefficient is 0.99.

Table 1 Grid characteristics

Grid no.	Mesh size (in.)	Rod diameter (in.)
0	No grid	
1	0.594	0.141
2	0.812	0.156
3	1.125	0.219

4. Experimental Method and Instrumentation

4.1 Aerodynamic Measurements

Flow measurements of the mean velocity in the axial direction and the turbulence intensity in the axial and circumferential directions were made with an x-configuration hot-wire probe. The probe was traversed radially along the blade span; measurements were taken at eight radial locations and 0.64 chord lengths upstream of the rotor, as shown in Fig. 2. In addition, these radial traverses were made at three circumferential positions, 90° apart.

The axial velocity or flow coefficient was controlled by the Joy axial flow fan, located downstream of the compressor as shown in Fig. 1. The turbulence intensities and longitudinal integral length scales of the turbulence were varied by the use of three square mesh grids placed 2.65 chord lengths upstream of the rotor, as shown in Fig. 2. Table 1 gives the grid mesh sizes and rod diameters.

The approximate longitudinal integral length scale of the turbulence has been experimentally measured using a hot-wire probe. The sensor was positioned normal to the flow direction; measurements were made at three radial positions. The autocorrelation function was obtained by using a correlation computer. The length scale was then approximated from the measured temporal integral scale and the axial mean flow velocity. The axial component of the turbulent energy spectrum was measured at the midspan of the rotor; measurements were made behind the three grids and with the open duct for all three rotor rpm's.

4.2 Acoustic Measurements

Acoustic measurements of the sound field produced by the compressor were made while it was operated at different flow coefficients and with various inlet turbulence intensities and length scales. Both narrow band 10 Hz and ⅓-octave band sound pressure level (SPL) spectrums of the noise were obtained. In addition, the directivity of the sound field was filtered and measured by the ⅓-octave band wave analyzer. The total power radiated from the compressor was derived from additional measurements.

A ⅛-in. Bruel & Kjaer condenser microphone was positioned on the compressor axis at distances of 4.35 and 8.7 duct diam from the inlet, as shown in Fig. 2. Both 10 Hz and ⅓-octave wave analyzers were employed to filter the signal. A Graphic level recorder was attached to the filter output and provided a permanent record of the sound pressure spectrum.

The directional characteristics of the sound field produced by the compressor were obtained from SPL measurements made in a horizontal plane in an arc from the 0° station, on the compressor axis, to the 90° station, in the plane of the compressor inlet (Fig. 2). These measurements were made in 5° increments; the distance between microphone and compressor inlet was 4.35 duct diam. The signals were filtered by a ⅓-octave wave analyzer and recorded on a chart recorder.

The sound power was then obtained by positioning the B & K microphone at twelve equally spaced locations on

Table 2 Summary of aerodynamic and acoustic measurements

Grid no.	rpm	Values at midradius U_{rel}(fps)	$(\overline{u^2})^{1/2}/U_x$	$(\overline{v^2})^{1/2}/U_x$	Λ_f/S	ϕ	$((\overline{g^2})^{1/2}/\Lambda_f)_{max}$	PWL(db)
0	3626	127.2	0.020	0.030	...	1.19	...	88.7
(No grid)	4360	153.2	0.005	0.020	...	1.19	...	86.9
	5440	186.4	0.019	0.025	...	1.14	...	89.6
1	3626	127.5	0.035	0.080	0.269	1.20	414.	89.8
	4360	153.8	0.020	0.045	0.237	1.20	273.	87.6
	5440	187.3	0.021	0.050	0.400	1.15	169.	90.6
2	3626	129.8	0.035	0.090	0.241	1.23	404.	92.7
	4360	145.8	0.025	0.050	0.212	1.10	280.	93.5
	5440	182.9	0.025	0.060	0.300	1.16	340.	95.0
3	3626	134.0	0.035	0.095	0.234	1.30	456.	93.2
	4360	154.5	0.030	0.075	0.239	1.21	390.	93.5
	5440	182.0	0.038	0.090	0.286	1.09	479.	97.4

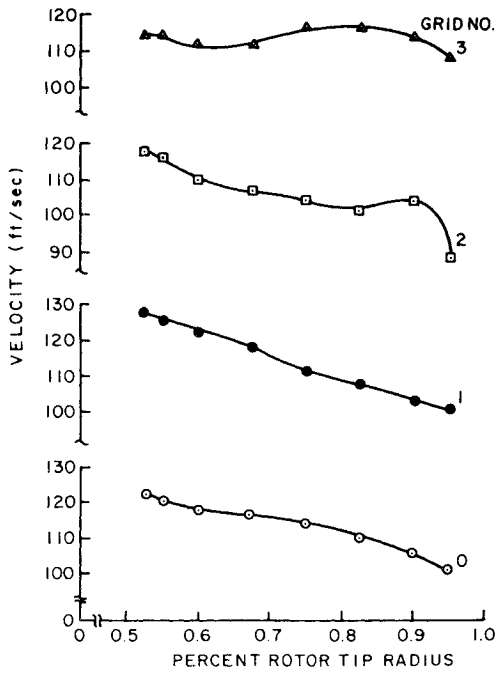

Fig. 3 Measured inlet mean velocity profiles. Rotor operated at 4360 rpm.

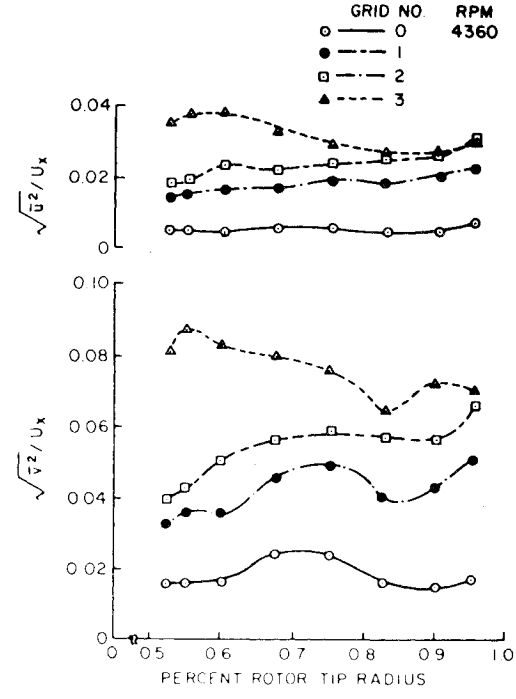

Fig. 4 Measured inlet axial and circumferential turbulence intensities. Rotor operated at 4360 rpm.

the surface of a quadrant of a hemisphere surrounding the inlet. Also, the average SPL obtained over the quadrant was later used in deriving the directivity gain index. A ⅓-octave band analyzer connected to a chart recorder was again used in these measurements.

5. Experimental Results

In this section, we quote only the typical results, for a complete set of results the reader is referred to Ref. 10.

5.1 Aerodynamic Measurements

The results of the mean velocity (absolute) measurements are shown in Fig. 3. The velocity profiles of the flow in the axial direction indicated at least a 15% variation in velocity between the hub and tip of the rotor. Clearly, the local flow coefficient is larger near the hub than at the blade tip. The average flow coefficient for the different operating conditions is given in Table 2. This average flow coefficient is defined as the ratio of the mass averaged axial velocity to the blade speed at midradius.

Figure 4 shows the results obtained for the turbulence intensities in the axial and circumferential directions. Note that the value of the circumferential component $(\overline{\mu^2})^{1/2}/V_x$ is about twice the value of the axial component $(\overline{u^2})^{1/2}/V_x$. Thus, the turbulence is nonisotropic, even though it is nearly uniform from hub to tip. The turbulence interacting with the rotor is nonisotropic due to the close proximity of the rotor to the grid. Since the rotor is only a few mesh sizes downstream, the turbulence has not fully developed.

Values of the longitudinal integral length scale of the turbulence were found to vary from 0.2 to 0.4 in. across the annulus in front of the rotor. The integral scale Λ_f nondimensionalized by the local blade spacing S is tabulated in Table 2, and graphically shown in Fig. 5. Λ_f is found to be nearly constant across the annulus, even though the ratio decreases towards the tip due to larger blade spacing at that location.

The turbulent energy spectrum of the axial component of the fluctuating velocity was obtained for all operating conditions. As typical of the results, Fig. 6 shows the spectrums obtained behind grid number 3 and with the open duct (no grid). With the open duct the energy spectrum drops 35 db between 0 and 4,000 Hz; with Grid No. 3 the spectral decline is only 13 db in the same frequency range. The frequency at which the slopes of the two spectrums are the same occurs around 2,000 Hz.

Thus, the turbulence that was generated by the grid has not decayed substantially at the higher frequencies. The grid turbulence spectrum has a small slope; this would produce an acoustic spectrum with the same characteris-

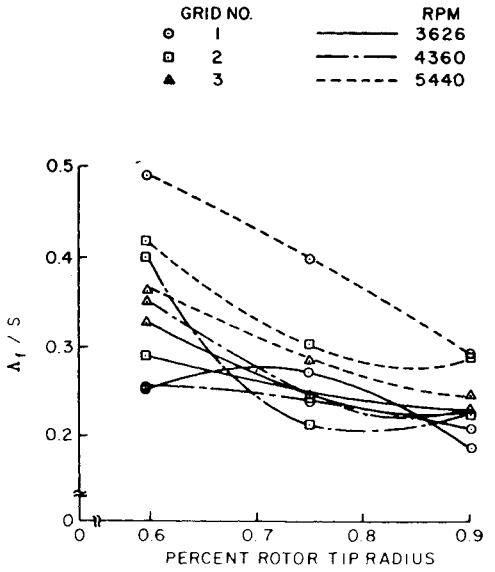

Fig. 5 Measured inlet nondimensionalized longitudinal integral length scale of the turbulence.

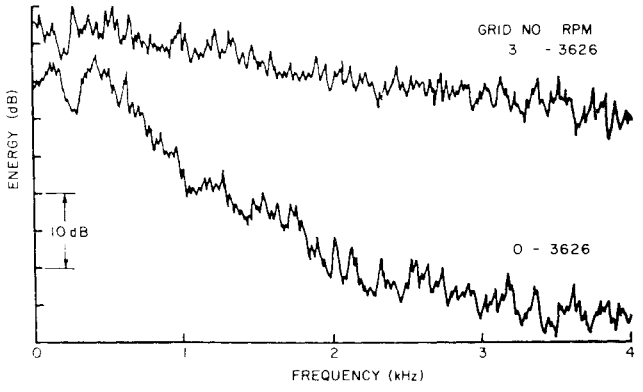

Fig. 6 Measured axial component of the turbulent energy spectrum.

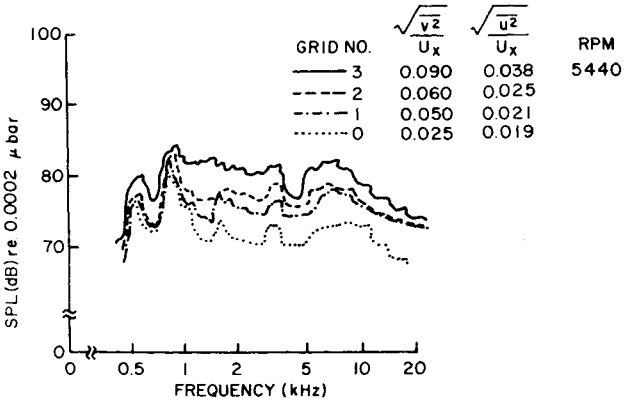

Fig. 7 Effect of turbulence intensity on the spectrum of the sound pressure level.

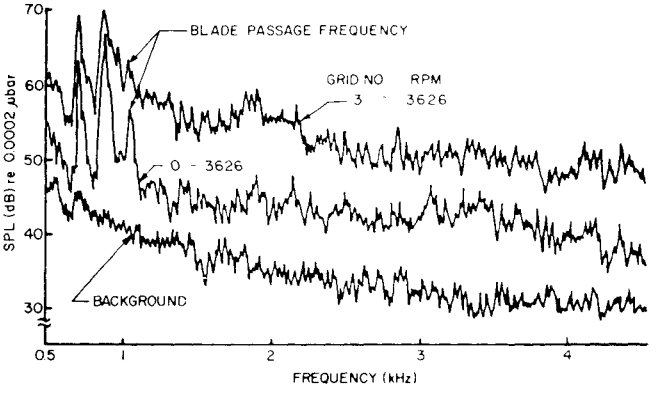

Fig. 8 Typical narrow band sound pressure level spectrum.

tic shape. On the other hand, the open duct spectrum has more energy at the lower frequencies and would produce an acoustic spectrum with this basic characteristic.

5.2 Acoustic Measurements

The results of the acoustic measurements shows an increase in the sound pressure level with an increase in turbulence intensity. Figure 7 shows the ⅓-octave band measurement of the spectrum level of the sound pressure at various inlet turbulence levels, averaged from hub to tip in the free steam. These results were obtained with the microphone located on the compressor axis at a distance of 30 in. (or 4.35 duct diam) from the inlet; the rotor was operated at 5440 rpm. Grid No. 0 denotes no grid in the duct, the corresponding turbulence intensity was found to be small. Upon placing a grid in the inlet flow, both turbulent velocity components increase, thus adding to the acoustic radiation via the unsteady blade forces. Similar increases in the spectral level occur with the other two grids. In addition to the variation of turbulence intensity, the integral scale also varied as seen in Table 2. The effect of the integral scale variation will be discussed later.

Figure 8 shows a comparison of the narrow band sound measurements of the background noise (equipment turned on, compressor turned off) and the sound spectrums with the rotor operating at 3626 rpm in an open duct (no grid) and with Grid No. 3. It is clear from this figure that the background noise is lower than the lowest sound spectrum level generated by the compressor (no grid and 3626 rpm). The spectrum represents the true spectral level of the compressor, with little influence from the background noise. Comparing spectral levels, the spectrum from Grid No. 3 is always 10 db greater than the background noise at all frequencies. This confirms the extent of turbulence induced noise.

The BPF at this rotor speed is 1028 Hz. As seen from Fig. 8 a peak occurs at this frequency in the spectrum of the rotor with Grid No. 3. Also noticeable are the peaks occurring at 750 and 900 Hz; these occur at all the operating conditions. It is felt that these are caused by vibrations in the microphone supports. Therefore, these peaks have no acoustic relevance.

The directivity patterns of the SPL of the broadband noise were found to exhibit directional properties, as typified by Fig. 9. This figure shows the effect of turbulence intensity on the directional properties of the radiated sound. The graph indicates a circular pattern from 0° to 50° off the compressor axis. From 50° to 90° stations, a substantial decrease of 12 db was observed. The directional dependence of the broadband noise occurs in the solution of the wave equation. By choosing the appropriate Green's function which applies to the far-field, the solution is found to depend on the angle between the observer and the compressor axis.

Both Sevik and Mani predict (Eqs. (1) and (4), respectively) that the turbulence induced noise should be proportional to (turbulence intensity).[2] Furthermore, for small values of Λ_f, F_1 in equation 1 is nearly independent of Λ_f and hence Sevik's theory predicts the SPL to be proportional to $(\Lambda_f)^{-2}$. Mani's expression [Eq. (4)] also indicates that, for small values of Λ_f, *SPL* should vary as $(\Lambda_f)^{-2}$. These in addition to Sharland's Eq. (8) indicate that

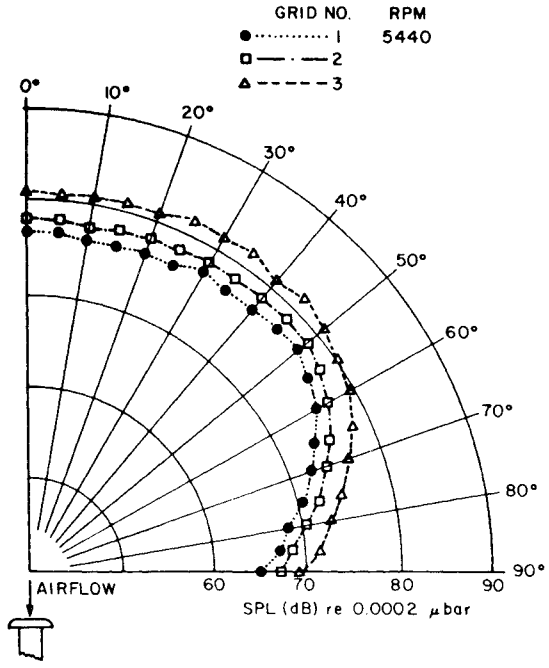

Fig. 9 Typical measured SPL of broadband noise from ⅓-octave analysis.

$$SPL \text{ or } PWL \sim \left(\frac{(\overline{u^2})^{1/2}}{\Lambda_f}\right)^2 U_{\text{rel}}{}^4$$

Since the turbulence is nonisotropic in our case, the logical choice for the turbulence velocity is the mean square value normal to the blade chord given by

$$\overline{q^2} = \overline{v^2}\cos^2\xi + 2\overline{uv}\sin\xi\cos\xi + \overline{u^2}\sin^2\xi \qquad (9)$$

In addition, the spanwise effects are important. The effective radius is the one which has the maximum lift fluctuations. Since the rotor used in this investigation is of free vortex design (constant blade loading from hub to tip in steady flow), the maximum lift fluctuations occur at the spanwise location where $(\overline{q^2})^{1/2}/\Lambda_f$ is maximum. Hence

$$SPL \text{ or } PWL \sim \left(\frac{\overline{q^2}}{\Lambda_f}\right)_{\text{MAX}} U_{\text{rel}}{}^4 \qquad (10)$$

where U_{rel} is the relative velocity at the spanwise location where $(\overline{q^2})^{1/2}/\Lambda_f$ is maximum.

The total sound power (PWL), derived from the SPL measurements and integrated over a sphere of radius 2.5 ft, is plotted against $\overline{q^2}U_{\text{rel}}{}^4/\Lambda_f{}^2$ in Fig. 10 and tabulated in Table 2. This plot clearly confirms the validity of Eq. (10). Hence

$$PWL = PWL_0 + 40\log U_{\text{rel}} + 10\log\overline{q^2} - 20\log\Lambda_f \qquad (11)$$

where U_{rel} and $(q^2)^{1/2}$ are in fps and Λ_f is the integral length scale in ft. PWL_o is a constant base level, for this rotor its value is −45.2 db. The scatter of the experimental data is within ±1.5 db of the relationship given by expression 11, plotted in Fig. 10; the accuracy of these measurements is ±1 db.

This clearly establishes the fact that the turbulence induced noise depends not only on the maximum turbulence intensity (normal to the blade chord), but also on the scale of the turbulence. This is one of the important quantitative conclusions of this investigation. The relationship [Eq. (11)] is valid for turbulence integral length scales smaller than the blade spacing. If they are of the same order of magnitude or higher, one may expect the turbulence induced noise to be a complicated function of Λ_f as predicted by Sevik and Mani.

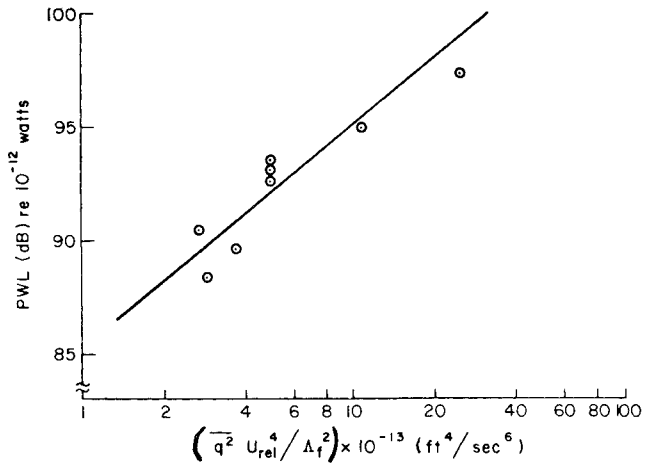

Fig. 10 Variation of PWL with relative flow velocity, turbulence intensity, and integral length scale.

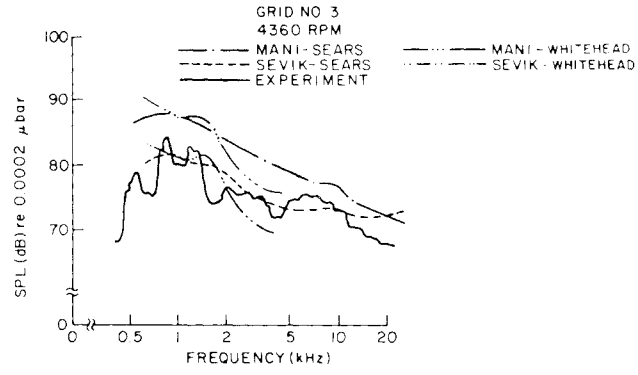

Fig. 11 Comparison of predicted spectrum with measured spectrum of SPL (⅓ octave analysis).

5.3 Comparison of Experiment with Theory

The theories of Sevik and Mani (Sec. 2) both with the Sears function $S(\omega)$ and with the cascade function of Whitehead $[H(\omega,\sigma,\xi)]$ are used to compute the spectrum levels of the sound pressure for the compressor used by the authors. The comparison between the measured SPL and calculated sound power levels was made by converting Sevik's prediction to SPL values. Details of this calculation can be found in Ref. 10.

The predictions are compared with the experimental results in Fig. 11, which shows the ⅓ octave results of the sound spectrums obtained for the rotor at 4360 rpm with Grid No. 3. In this figure the Sevik-Sears predictions are quite good; the Mani-Sears predictions overestimate the experimental results by about 6 db, especially at low frequencies. The Sears function, $S(\omega)$, is found to be slightly lower than the Whitehead's function $C_{FW}(H(\omega,\sigma,\xi)$ in our notation) for frequencies up to 2 KHz. Beyond this, the trend was reversed and the unsteady loads in a cascade of blades are found to be lower than that of an isolated blade with the same relative velocity. This is reflected in the SPL predictions plotted in Fig. 11. Sevik-Sears and Sevik-Whitehead predictions are found to be nearly the same up to 2 KHz, beyond which a maximum of 4 db discrepancy is observed between the two calculations. Mani-Whitehead predictions seem to fall closer to experimental values at higher frequencies. The cascade function, $H(\omega,\sigma,\xi)$, from Whitehead's analysis[8] could not be calculated beyond 4 KHz due to numerical convergency problems.

Narrow band comparisons indicate that the Sevik-Sears theory accurately predicted the spectrum level of the sound pressure from 3,000 to 10,000 Hz. Above and below this range of frequency, Sevik's calculations overestimate

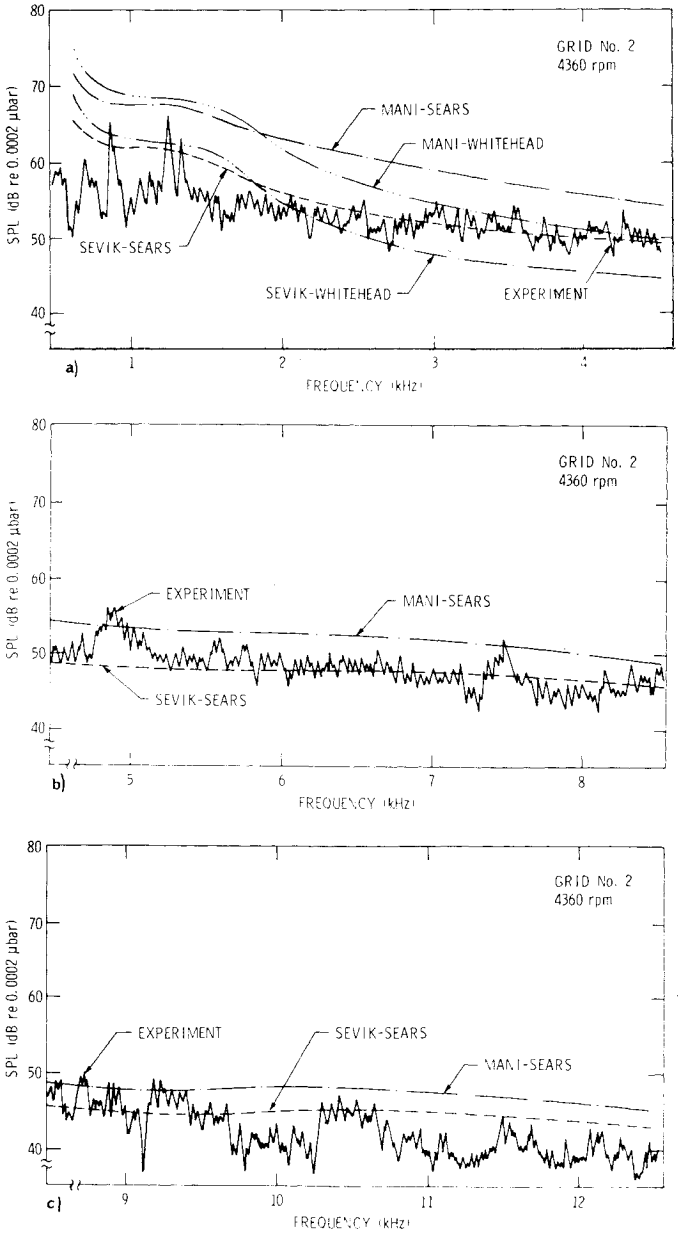

Fig. 12 Comparison of predicted spectrum with measured spectrum of SPL (narrow band analysis).

the experimental results (Fig. 12a-c). Sevik[3] states that "The predicted spectrum level becomes inaccurate at values of $\Lambda_f/\lambda > 0.25$, since the integral scale of the turbulence and the wavelength of the sound become comparable magnitude." Sevik's analysis becomes increasingly inaccurate when Λ_f and λ are of the same order of magnitude, since the retarded time changes in the derivation of noise level is not negligible. Hence in the present experiment, Sevik's theory is valid up to about 10 KHz. One criticism of Sevik's theory is that it does predict the blade passage frequency.

Although Mani's analysis is general enough to predict an increase or peak in the sound spectrum level at BPF and higher harmonies, these peaks represent a concentration of coherent broadband energy at those frequencies. In this study, no peaks were predicted by Mani's analysis (Figs. 11 and 12a). Physically, as the integral scale gets smaller, the band width of the turbulent eddy source frequencies broaden and the corresponding acoustic frequencies produce broad band noise. On the other hand, if the rotor chops through the large eddies (large integral scale) the turbulent source frequency band width is small and thus a peak occurs at the BPF.

Mani has theoretically shown the effect of Λ_f/S on the level of the sound spectrum. His results indicate a decrease in the spectrum level of 5 db with an increase in the value of Λ_f/S by a factor of 4. Referring to Fig. 5, the experimental value of Λ_f/S varied by a factor of 2 over the blade span. This, together with the experimental error in measuring the integral scale, would account for, at least, 4 db in the Mani-Sears overestimate of the spectrum level. Physically, as Mani explains it, for large values of Λ_f/S the turbulence appears to the rotor as a stator blade row with very few vanes (relative to the rotor blade number); thus, most of the interactions produced are spinning too slowly in the duct to effectively propagate. With decreasing values of Λ_f/S, greater portions of the turbulent kinetic energy spectrum participate in the noise production process.

6. Conclusions

The following conclusions can be drawn from the noise studies conducted with a single-stage compressor operated over a range of tip speeds with various inlet turbulence characteristics, such as intensity, energy spectrum, and integral length scale.

1) The total sound power is dependent not only on the intensity but also on the scale of the turbulence. For integral length scales smaller than the blade spacing, the total sound power is found to be proportional to (turbulence velocity/integral length scale),[2] where the turbulence velocity is the rms value normal to the blade chord. Total sound power is also found to be proportional to U_{rel}.[4] The expression

$$\text{PWL} = \text{PWL}_0 + 40 \log U_{\text{rel}} + 10 \log \overline{q^2} - 20 \log \Lambda_f$$

seems to provide predictions which are in close agreement with the experiment. These conclusions are in agreement with the predictions of Mani, Sevik and Sharland.

2) The sound spectrum has a shape that is similar to the shape of the turbulent energy spectrum. Large amounts of broadband noise in the sound spectrum corresponds to relatively large amounts of energy found in the turbulent energy spectrum.

3) The broadband radiation patterns exhibited a directional characteristic which is typical of compressors. The peak *SPL* usually occurred off the compressor axis.

4) The sound spectrum levels produced by the inlet distortions can be predicted over a limited frequency range. The overestimate of the Sevik-Sears prediction at lower frequencies can be attributed to his use of the Sears function for the unsteady lift. It is felt that the interference effect on the unsteady lift between blades in a cascade is the cause of this deviation in theory from the experiment. Sevik's and Mani's theories with single airfoil unsteady lift calculations agree with experimental results at frequencies above 3,000 Hz. The predictions contain no peaks (except at BPF) in the spectrum, which is in contradiction with the measured spectrum.

5) The use of the cascade gust function did not affect the SPL prediction at moderate frequencies (0.7 to 2KHz). At higher frequencies, the predictions with cascade gust function came closer to experiment, especially with Mani's theory.

References

[1]Ffowcs-Williams, J. E. and Hawkings, D. L., "Theory Relating to the Noise of Rotating Machinery," *Journal of Sound and Vibration,* Vol. 10, No. 1, 1969, pp. 10-21.

[2]Chandrashekhara, N., "Sound Radiation from Random Qua-

drupole Source Distributions in Axial Flow Fans," *Journal of Sound and Vibration*, Vol. 19, No. 2, 1971, pp. 133.

[3]Sevik, M., "Sound Radiation from a Subsonic Rotor Subjected to Turbulence," *Proceedings of the International Symposium on Fluid Mechanics and Design of Turbomachinery*, Aug. 31–Sept. 4, 1970, The Pennsylvania State University, University Park, Pa. (To be published as NASA SP 304, 1974.)

[4]Mani, R., "Noise Due to Interaction of Inlet Turbulence with Isolated Stators and Rotors," *Journal of Sound and Vibration*, Vol. 17, No. 2, 1971, pp. 251–260.

[5]Sears, W. R., "Some Aspects of Non-Stationary Aerofoil Theory and Its Practical Application," *Journal of the Aeronautical Sciences*, Vol. 8, No. 3, 1941, pp. 104–108.

[6]Sofrin, T. G. and McCann, J. C., "Pratt and Whitney Experience in Compressor Noise Reduction," Presented at the 72nd Meeting of the Acoustical Society of America, 1966.

[7]Hanamura, Y., "Flutter of Cascading Blade Row," Rept. 459, 1971, Institute of Space and Aero Sciences, University of Tokyo, Tokyo, Japan.

[8]Whitehead, D. S., "Force and Moment Coefficients for Vibrating Aerofoils in a Cascade," R & M 3254, 1960, Aeronautical Research Council, London, England.

[9]Sharland, I. J., "Sources of Noise in Axial Flow Fans," *Journal of Sound and Vibration*, Vol. 1, No. 3, 1964, pp. 302–322.

[10]Robbins, B., "Turbulence Induced Noise in a Single Stage Axial Flow Fan," M. S. thesis, 1974, Department of Aerospace Engineering, The Pennsylvania State University, University Park, Pa.

MAY 1974 J. AIRCRAFT Vol. 11, No. 5

Passage of a Swept Airfoil through an Oblique Gust

John J. Adamczyk*
United Aircraft Research Laboratories, East Hartford, Conn.

An analysis is presented which yields an approximate solution for the unsteady aerodynamic response of an infinite swept wing encountering a vertical oblique gust in a compressible stream. The approximate expressions are of closed form and do not require excessive computer storage or computation time, and further, they are in good agreement with the results of exact theory. This analysis is used to predict the unsteady aerodynamic response of a helicopter rotor blade encountering the trailing vortex from a previous blade. Significant effects of three dimensionality and compressibility are evident in the results obtained.

Nomenclature

a	= speed of sound
C	= cosine Fresnel integrals
E	= complex Fresnel integral, defined by Eq. (25)
H_0, H_1	= Hankel functions, first kind, orders 0 and 1
I_0, I_1	= modified Bessel functions, first kind, order 0 and 1
J_0, J_1	= Bessel functions, first kind, orders 0 and 1
K	= gust wave number
M	= Mach number of the freestream, U/a
n	= integer
r	= radial distance from the midchord line of the airfoil
R	= dimensionless radial distance
S	= sine Fresnel integral
t	= time
$\overline{u_2}$	= complex amplitude of u_2'
x_i	= Cartesian coordinates, Fig. 1
X_i	= dimensionless coordinates, defined by Eqs. (9) and (10)

Subscript

1/4	= quarter-chord

Introduction

THE determination of the unsteady aerodynamic response of an airfoil to a vertical gust velocity field has long been of interest to aeroelasticians and acousticians. For the most part aeroelasticians have used the incompressible two-dimensional theories of Kussner[1] and Sears[2] to predict the unsteady response. In estimating the acoustic field generated by airfoil-gust interactions the acoustician typically uses the unsteady lift obtained from one of the previous theories to determine the strength of the acoustic dipole source which is then assumed to replace the airfoil in the flowfield (e.g., Curle in Ref. 3).

Typical of the many unsteady aerodynamic problems in which these incompressible theories have been used in the past are: 1) rotor blades passing through the wakes of stator blades in turbomachinery, 2) an airfoil interacting with a turbulent gust, and 3) helicopter rotor blades encountering the tip vortices from proceding blades. In each of these problems some uncertainty arises as to the applicability of two-dimensional incompressible aerodynamics. It is not surprising, therefore, that several analytical studies have appeared recently which treat the complexities of three dimensionality and compressibility in the unsteady problem. For example, Filotas[4] obtained a closed form solution for an oblique sinusoidal gust encountering an infinite wing; however, this work is limited to a two-dimensional airfoil of zero sweep (i.e., the incoming flow is normal to the leading edge line of the wing) in an incompressible stream. Graham[5] included the effects of compressibility and three dimensionality but neglected the effects of sweep. His analysis is based on a numerical solution of the governing differential equations. Adamczyk[6,7] also included the effects of compressibility and three dimensionality, but the form of the solution was expressed in terms of an infinite series of Mathieu functions which are difficult to evaluate analytically. Another recent analysis by Johnson[8] included the effects of compressibility and three dimensionality; however, his approach is tailored towards analyzing the response of an airfoil to a free rectilinear vortex. Hence, the researcher has had no simple compressible three-dimensional analogue of the Sears solution available to him and was required to resort to the more restricted theories of Filotas

Presented as Paper 73-683 at the AIAA 6th Fluid and Plasma Dynamics Conference, Palm Springs, Calif., July 16–18, 1973; submitted August 13, 1973; revision received January 22, 1974. This work was supported by NASA Langley Research Center and USAAMRDL-Langley Directorate under Contract NAS1-11557.

Index categories: Nonsteady Aerodynamics; Aircraft Gust Loading and Wind Shear; Rotary Wing Aerodynamics.

*Research Engineer, Aeroelastics Group.